

## A small electron cyclotron resonant plasmabased neutralflux ionizer

B. L. Cain and D. N. Ruzic

Citation: *Rev. Sci. Instrum.* **61**, 3473 (1990); doi: 10.1063/1.1141606

View online: <http://dx.doi.org/10.1063/1.1141606>

View Table of Contents: <http://rsi.aip.org/resource/1/RSINAK/v61/i11>

Published by the [American Institute of Physics](#).

---

### Related Articles

Perpendicular and tangential angularly resolved multi-sight neutral particle analyzer system in LHD  
*Rev. Sci. Instrum.* **83**, 10D920 (2012)

Invited Article: Relation between electric and magnetic field structures and their proton-beam images  
*Rev. Sci. Instrum.* **83**, 101301 (2012)

Enhanced NIF neutron activation diagnostics  
*Rev. Sci. Instrum.* **83**, 10D315 (2012)

Development of a diagnostic technique based on Cherenkov effect for measurements of fast electrons in fusion devices  
*Rev. Sci. Instrum.* **83**, 083505 (2012)

Neutron activation diagnostics at the National Ignition Facility (invited)  
*Rev. Sci. Instrum.* **83**, 10D313 (2012)

---

### Additional information on *Rev. Sci. Instrum.*

Journal Homepage: <http://rsi.aip.org>


Journal Information: [http://rsi.aip.org/about/about\\_the\\_journal](http://rsi.aip.org/about/about_the_journal)

Top downloads: [http://rsi.aip.org/features/most\\_downloaded](http://rsi.aip.org/features/most_downloaded)

Information for Authors: <http://rsi.aip.org/authors>

## ADVERTISEMENT

**JANIS** Does your research require low temperatures? Contact Janis today.  
Our engineers will assist you in choosing the best system for your application.



10 mK to 800 K  
Cryocoolers  
Dilution Refrigerator Systems  
Micro-manipulated Probe Stations

LHe/LN<sub>2</sub> Cryostats  
Magnet Systems

[sales@janis.com](mailto:sales@janis.com) [www.janis.com](http://www.janis.com)  
Click to view our product web page.

# A small electron cyclotron resonant plasma-based neutral-flux ionizer

B. L. Cain<sup>a)</sup> and D. N. Ruzic

Department of Nuclear Engineering, University of Illinois, 214 NEL, 103 South Goodwin Avenue, Urbana, Illinois 61801

(Received 14 May 1990; accepted for publication 18 July 1990)

The design and operation of a neutral-hydrogen flux detection system is described. The central feature of the detector is an inductively driven electron cyclotron resonance heated (ECRH) discharge, which functions as the neutral-flux ionizer. The prominent features of the ionizer are its small ( $5 \times 3 \times 3$  cm<sup>3</sup>) size and excitation of the ECRH mode using a 200-W, 30-MHz rf driver and static magnetic field level near 30 G. The ability of the system to ionize 910-eV neutral-hydrogen fluxes with subsequent detection in a high resolution energy analyzer is shown. The detection efficiency of the ionizer was found to be  $\approx 6 \times 10^{-4}$ , based on scattering and charge exchange cross sections measured using a methane charge exchange cell. The ionizer has potential applications in angle-resolved reflected neutral-flux measurements and in beam-plasma interaction analysis.

## I. INTRODUCTION

The interaction of low energy hydrogen ions and charge exchange neutral fluxes with material surfaces and plasma sheaths is a prominent physical phenomenon in the edge regions of both magnetic fusion devices and plasma devices used in microelectronics processing.<sup>1-5</sup> For incident energies below 1 keV, collision of these particles with surfaces produces a backscattered or reflected flux often dominated by neutral particles. The energy, angle, and species distributions of this reflected flux embodies much of the fundamental information regarding the ion-surface interaction, and they also influence the local plasma sheath structure. The importance of these interactions has been well addressed in several experimental and theoretical investigations,<sup>6-11</sup> yet the capability to better analyze low-energy neutral-atom fluxes remains a key factor in evolving the understanding of this fundamental phenomenon.

The objective of this research was the demonstration of an in-vacuum neutral-atom detection system capable of analyzing low-energy neutral-hydrogenic particles at flux intensities typically encountered in a beam-surface reflection measurement.<sup>12</sup> To simulate these fluxes, and to provide a means for estimating the neutral-flux intensity for calibration purposes, a 910-eV H<sub>1</sub><sup>+</sup> ion beam was focused through a methane charge exchange cell onto the entrance of a small ECR driven discharge ionizer, with subsequent focusing and energy analysis of the re-ionized hydrogen flux. These ions were then detected using a dual channel plate coupled to standard counting electronics. The system was calibrated by first measuring angular charge exchange cross sections for the H<sub>1</sub><sup>+</sup> on CH<sub>4</sub> in the exchange cell, then using these cross sections to estimate the neutral-hydrogen flux incident on the ionizer. The ECRH discharge was of interest due to successes in Sputtered Neutral Mass Spectroscopy (SNMS), which applies a similarly designed discharge for sputtered-neutral-flux ionization.<sup>13-15</sup> The ECRH type discharge was selected because

of its high ionization efficiency at relatively low gas pressures, and its potential for obtaining a small ionizer volume for angle-resolved measurement capability.

## II. EXPERIMENTAL FACILITY

The pumping system and major experiment components, shown in Fig. 1(a), consists of a Colutron ion gun,<sup>16,17</sup> differentially pumped beamline, and a main chamber which houses raster/decel lenses, the target area, and the ECRH ionizer/analyzer combination. Details of the ion gun and the raster/decelerator stage have been covered in an earlier publication.<sup>18</sup> The main chamber is a 60.96 cm (diameter)  $\times$  45.72 cm (high) stainless-steel ultra-high vacuum chamber with 24 flanged ports for pumping and feedthrough access. The chamber is bakable to 200 °C using custom heating bands around the chamber diameter, along with an insulated bakeout shroud. The pumping system is instrumented with various thermocouple and ion gauges which are relay connected to a special ac-power control unit providing fail-safe operation of the vacuum system. Ultimate pressures in the system are  $10^{-9}$  Torr in the main chamber,  $10^{-8}$  Torr at the differentially pumped beamline, and  $5 \times 10^{-8}$  Torr in the gun chamber.

The main chamber geometry, Fig. 1(b), shows the design placement of experiment components for a reflected-neutral-flux measurement. To maximize the viewing solid angle, and to allow rotation of the ionizer/analyzer within the chamber, the ionizer was kept as small as possible. In this work, the ionizer was rotated to the straight-through alignment with the raster/decel stage, and the target was replaced with a small stainless-steel gas cell mounted on an XYZ $\theta$  manipulator. A 5° beamline deflection between the ion gun and the main chamber, which dumps beam neutrals in the cryo-pumped beamline, was included to enhance differential pumping between the gun and the main chamber. The pressure baffle and dual pumping on the main chamber was installed to provide a decade pressure

<sup>a)</sup>Presently at Mississippi State University, Mechanical and Nuclear Engineering Department, P. O. Drawer NE, Mississippi State, MS 39762.

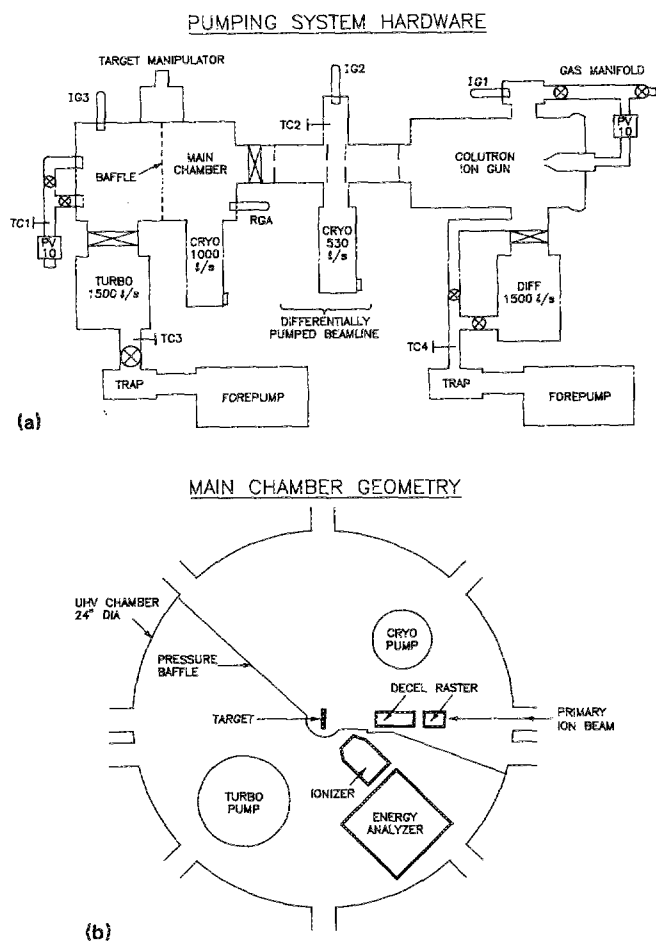


FIG. 1. (a) Ion gun and main-chamber pumping system hardware. (b) Main chamber geometry. In this work, the ionizer and analyzer were rotated about the target area to be aligned with the primary ion beam.

differential between the ionizer and the target region. With the primary ion beam on and ionizer gas flowing, the pressure on the target side of this baffle could be maintained near  $10^{-8}$  Torr.

The ion beam was produced from a dc arc discharge maintained with hydrogen gas at approximately 1 mTorr between a biased hot filament and anode plate in the gun source chamber. The source pressure was held constant by a piezoelectric-valved pressure controller. The beam was extracted, and energy controlled, by a 900-V bias between an aperture (0.508 mm) in the anode plate and a grounded extraction electrode located 5 mm from the aperture. The extracted beam was focused through an einzel lens, velocity filter, and collimating apertures into the differentially pumped beamline of Fig. 1. Deflection plates were then used to steer the mass resolved and focused beam into the main chamber for final focus in the raster/decel lenses. The  $H_1^+$  beam species was verified by calibrating the velocity filter using both He and Ar trace gases in the source discharge. Energy analysis of the primary beam showed its true energy to be 910 eV, with an energy spread  $<0.5$  eV. This additional 10 eV beam energy is due to the plasma potential between the anode and discharge in the gun source chamber. A Faraday cup and beam profiling probe, mounted on the manipulator in the main chamber, were

used to monitor beam intensity and to maintain the unrastered beam spot focus at  $<0.5$  mm. The raster plates were then used for final beam steering and illumination of the gas cell entrance aperture. The raster system was normally set to a video mode, producing a scan frequency of 5 kHz on the  $x$  plates, and 22.7 Hz on the  $y$  plates. The raster capability allowed any changes in the beam focus to be effectively averaged over the target area, providing a uniform illumination. The focused and rastered beam could also be used to image the target by ac coupling to the target signal, and using this signal to intensity modulate an oscilloscope phase locked to the  $x$ - $y$  raster scan. Additionally, a Faraday screen was installed around the target area to minimize interference from the ionizer rf and magnetic fields. With these arrangements, 900-eV  $H_1^+$  beam currents  $\approx 200$  nA could be maintained for periods of several hours.

### III. IONIZER AND DETECTOR SYSTEM

The application of an ECRH discharge as a neutral-flux ionizer relies on plasma electrons to impact ionize the neutral atom beam moving through the discharge volume. It is similar in concept to the electron impact ionizer, with chief advantages of a positive plasma potential and much higher ionization efficiency. Since the discharge requires no driving electrodes to sustain the discharge, discharge stability does not depend on plasma/surface interactions such as secondary electron emission which can vary with time. In addition, sputtering of surface material onto probes and apertures is minimized. Another important consideration is that the ionization efficiency increases with lower-energy neutral atoms, as they spend significantly more time in the ionization region. Potential limiting factors include the presence of a support gas and rf and static magnetic fields required for discharge operation, all of which must be adequately shielded from other experiment components. These same factors can also alter the energy distribution of the measured flux. Using an ECRH discharge, the requirement for minimized discharge size is further limited by the dispersion and resonance character of the discharge. There exists a minimum discharge length below which the resonant condition cannot be excited for a given electron temperature,  $T_e$ , density,  $N_e$ , and gas pressure values.<sup>19-21</sup>

The discharge chamber is shown in Fig. 2, also indicating the shape and orientation of the rf exciting coil, the static magnetic field,  $B_z$ , and the beamline axis. To excite the ECR mode, the chamber is placed inside the rf coil with the exit aperture centered on the  $X$ - $Y$  plane containing the rf ground point. When  $B_z$  is zero, rf current driven through the coil produces linearly polarized electromagnetic waves incident on the four sides of the discharge boundary. These waves are strongly attenuated by skin-effect absorption and do not propagate. When the static magnetic field is active and tuned to the electron cyclotron frequency, however, the EM waves driven by coil surfaces in the  $X$ - $Y$  planes become circularly polarized. These waves can propagate under special resonance conditions, effectively heating the plasma electrons. This mode of

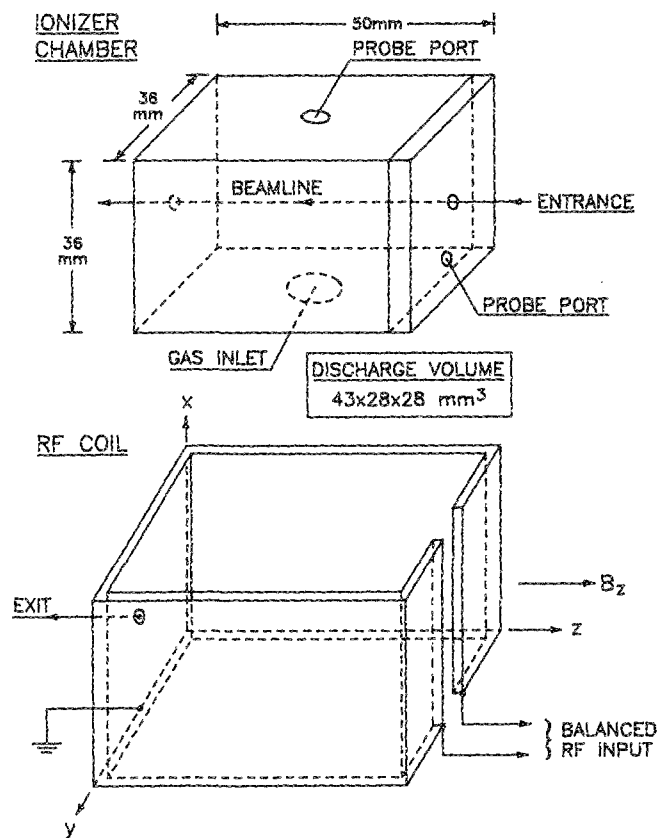


FIG. 2. ECRH ionizer chamber and rf-coil design with orientation of the beamline axis and static magnetic field,  $B_z$ .

propagation is well known in radio communication, and is often called the whistler mode.<sup>22</sup>

The ECRH discharge chamber and driver hardware were experimentally developed using successively smaller out-of-vacuum prototypes. With the resonance accessibility verified for an adequately small chamber, the in-vacuum version was constructed using high temperature ceramic, 304 stainless steel, and oxygen-free copper components. The basic chamber was machined from MACOR<sup>23</sup> ceramic with threaded fittings for attachment to a large Cu support plate, and for attachment of apertures and plasma probe access ports. The rf current coil, formed using a 5.08 mm (thick)  $\times$  2.54 cm (wide) Cu strap, was brazed to the support plate at the chamber exit. The balanced rf leads were brought out from the ionizer via custom rigid coaxial lines to a water-cooled, high-current rf feedthrough located in the bottom-center of the main chamber. Argon gas was supplied to the ionizer through a 2.54 cm (diameter)  $\times$  30.48 cm (long) flexible stainless bellows, which was brought out to a gas manifold instrumented with another piezoelectric-valved pressure controller and a Schulz-Phelps ionization gauge. Since the pressure gauge was located a considerable distance from the ionizer chamber, the ionizer pressure had to be inferred from a calibration done using formulas for gas-flow conductance and main-chamber pumping speed measurements.<sup>24,25</sup>

The axial magnetic field, aligned with the chamber beamline, was produced using a solenoid wrapped around

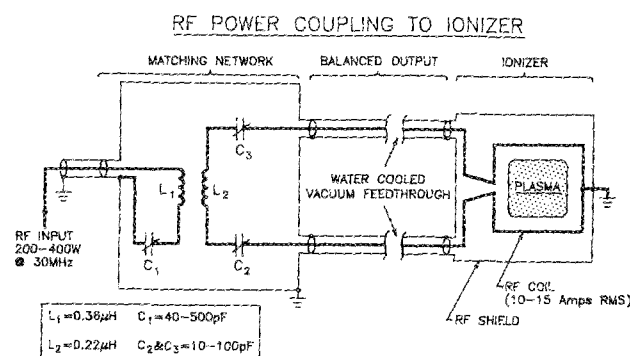


FIG. 3. Matching network used between rf amplifier and the grounded rf coil which drives the ionizer plasma.

a 6.35-cm (diameter) Cu support sleeve which fit just around the rectangular rf strap of Fig. 2. The coil was formed using 40 turns of 22-gauge Cu wire insulated with fiberglass sleeving, wrapped so that the coil extended past the apertures on both ends of the chamber. Due to the probe and gas ports located at the ionizer midplane, the final coil geometry was that of a split solenoid. The magnetic field strength along the ionizer axis was estimated to be 5 G per amp, with about 25% reduction in field strength at the entrance and exit aperture planes.<sup>26</sup> The rf and axial-field coils were then covered with an electrostatic shield made from Cu and stainless-steel screen materials bolted to the support plate.

The rf driver, shown schematically in Fig. 3, was constructed to series-resonate 30-MHz rf current through the network secondary and rf coil of the ionizer. The rf coil was grounded at the ionizer exit, providing the dc reference and minimizing rf voltages at the ionizer exit. The circuit was powered by an rf signal generator and a broadband, 50- $\Omega$  output, 500-W rf amplifier. Due to high VSWR in the balanced leads to the ionizer, significant power was lost due to heating of the rigid coaxial fittings and cabling. To minimize this loss, vacuum-insulated conductors were used for the in-vacuum lines, with air-insulated conductors for the out-of-vacuum lines. The network was capable of good matching over the range of 27-35 MHz, with reflected power typically  $<$  0.5 W for 200 W forward. A power level of 200 W was the power limit for the capacitors.

The energy analyzer used in this study was a spherical condenser, utilizing an inverse second power field between two spherical sectors to form the passed-energy trajectory.<sup>27-29</sup> It was operated in the constant transmission mode, and outfitted with entrance lenses and a fully enclosing Conetic magnetic shield box.<sup>30</sup> All beam-viewing surfaces were treated with a colloidal-graphite spray and polished to minimize surface charging. Apertures of 5 and 1 mm were used during the experiments, giving energy resolutions of 4.55% and 0.91%, respectively. These resolutions, and the analyzer transmission energy, were experimentally calibrated using traditional beam-scanning techniques,<sup>31</sup> and were found to be well within 5% of calculated values. The low-intensity energy-resolved flux from

DETECTOR, ENERGY ANALYZER, AND ENTRANCE LENS SCHEMATIC

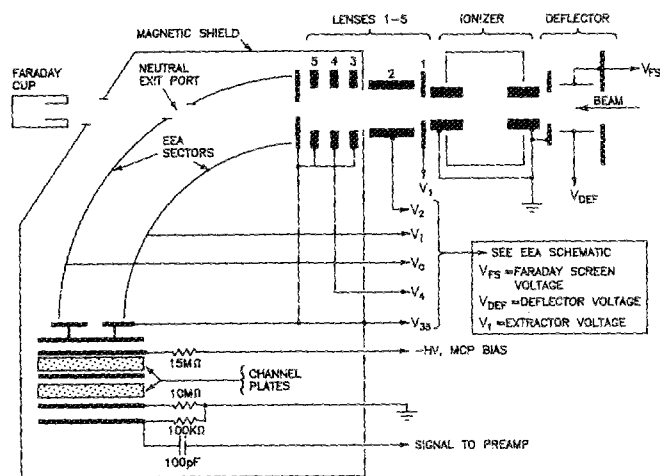


FIG. 4. Schematic arrangement of ionizer and energy analyzer.

the analyzer was detected using a channel-plate detector, operated in the pulse-counting mode.<sup>32,33</sup>

The arrangement of the ionizer and energy analyzer system is shown schematically in Fig. 4. The rf and magnetic-field coil leads are omitted from the drawing for clarity. The ionizer apertures were made from 0.478-cm (diameter)  $\times$  1.27-cm (long) stainless-steel tubing, to reduce gas loading external to the ionizer, and were electrically connected to system ground to fix the plasma space potential. The entrance to the ionizer was prefaced with deflector plates which could be biased to deflect plasma electrons and ions from backstreaming toward the target area. The plates could also be used to quench any beam metastable components. Similarly, an aperture lens,  $V_1$ , was used at the exit aperture to control escaping plasma particles.  $V_1$  was normally set to  $-100$  V, forming a potential barrier for electrons, and assisting extraction of plasma ions and re-ionized beam atoms. The potentials on the additional exit lenses (2-5 in Fig. 4) were experimentally adjustable to refocus the emerging ion flux into the energy analyzer aperture. For all energy-scan measurements, a 1-mm aperture was used at the analyzer entrance. A personal computer was used to control and monitor the voltages to the analyzer sectors and lenses, and to monitor the counting pulses from the channel plate. A straight-through "neutral-exit port" on the outer sector of the analyzer allowed the use of an additional Faraday cup for system alignment and beam intensity measurements when the analyzer was inactive and electrically grounded. This mode of detection was used for the beam attenuation and cross-section measurements.

IV. OPERATION AND CALIBRATION

The ionizer was started by first grounding all the components of the analyzer, then bringing the ionizer argon pressure up to  $\approx 100$  mTorr. With the rf power to the ionizer set to 200-W forward and the  $B_z$  field strength set near 30 G, high voltage ( $-1500$  V dc) was applied to a small tungsten probe installed at the ionizer midplane-

DISCHARGE ARGON ION ENERGY SCANS USING DIFFERENT TRANSMISSION ENERGIES

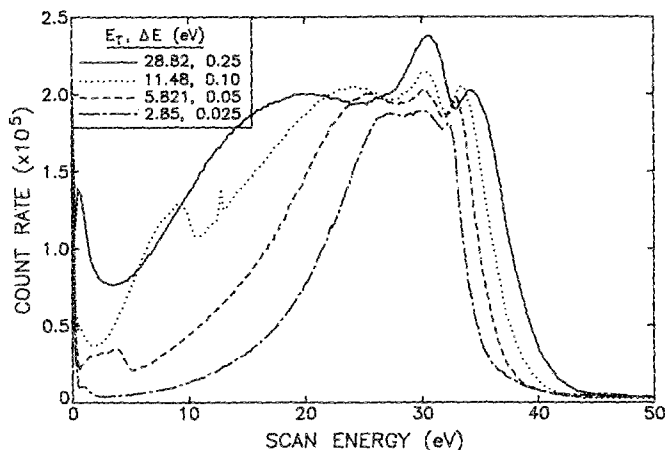


FIG. 5. Energy distributions of argon ions exiting ionizer aperture for various transmission energy,  $E_t$ , setting on the energy analyzer.

probe port. The discharge strike was detected by the electron signal collected on the Faraday cup of Fig. 4. Once the discharge was established, the gas pressure was slowly reduced while simultaneously adjusting the rf matching network for minimum reflected power. At pressures below 2 mTorr, the discharge could only be maintained by applying higher rf power, sustainable for only a few minutes due to capacitor breakdown in the matching network. By keeping the pressure constant near 5 mTorr, the ionizer could be operated essentially indefinitely. By continuously monitoring the plasma floating potential via the probe port near the ionizer entrance, stable plasma conditions could be conveniently verified during data collection periods which usually required several minutes.

At this stable operating point, energy scans of the discharge argon ions were obtained for a variety of different analyzer settings. Typical energy distributions are shown in Fig. 5, obtained for various analyzer transmission energies,  $E_t$ . The different shapes of the plots are due to "space-charge beam spreading" and defocusing effects in the ionizer exit lenses, which were expected since the beam energy is on the same order of magnitude as  $E_t$  for these scans. The true shape of the sampled ion distribution emerges as  $E_t$  approaches zero. The small peaks near 1 eV are apparently due to support-gas atoms ionized near the ionizer exit where the local sheath potential was small. Analysis of these curves shows the mean energy of the plasma ions to be  $28 \pm 2$  eV, with an energy width of  $12 \pm 3$  eV.<sup>12</sup> This width is believed to be equal to the difference between the maximum and minimum values of the time-varying plasma potential, and the mean energy is consistent with an "effective dc value" for the sheath potential encountered by the background ions upon exiting the discharge chamber.<sup>34-36</sup> Conventional Langmuir probe analysis of the plasma electron temperature and density,<sup>37,38</sup> taken from an out-of-vacuum prototype of this discharge at sim-

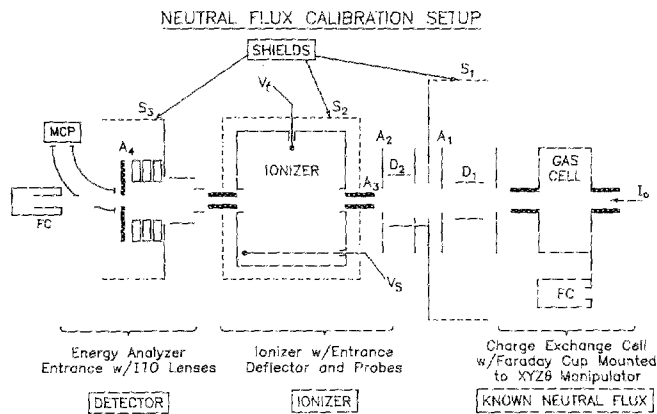


FIG. 6. Block diagram of apparatus used to measure cross sections and to estimate the flux of neutral atoms entering the ionizer.

ilar operating conditions, gave values of  $T_e \approx 7$  eV and  $N_e \approx 10^{11} \text{ cm}^{-3}$ , with error bars of 40% and 60%, respectively.

To determine the ionizer/analyzer efficiency for detecting low intensity hydrogen fluxes, the arrangement shown in Fig. 6 was used to produce a neutral-hydrogen beam by charge exchanging the  $\text{H}_1^+$  beam in the gas cell backfilled with  $\text{CH}_4$ . The deflector plates,  $D_1$  and  $D_2$ , were biased to remove primary beam ions and to deflect the ionizer ions/electrons, respectively. Apertures  $A_1$ – $A_4$  were carefully measured and aligned to establish the solid angles viewed by both the ionizer and the energy analyzer. The neutral-beam intensity was determined by measuring the charge exchange and scattering cross sections for two different angular apertures,  $A_4$ , then applying elastic scattering theory to the experimental cross sections to estimate the angular dependence of the charge-exchange cross section.<sup>12</sup> Neutral-hydrogen intensities  $\approx 5.0 \pm 2.7 \times 10^7$  ( $\text{H}_1^0/\text{s}$ ), passing through  $A_4$ , were obtained with this arrangement.

With the neutral-flux intensity established, the ionizer was operated at an argon gas pressure of 5 mTorr,  $B_z$  field of 30 G, and 200-W rf forward power at 30 MHz. Energy scans were then made of the ion flux from the ionizer, as shown in Fig. 7. For these distribution measurements, the methane pressure in the gas cell was varied from 1–12 mTorr, and the primary beam deflectors,  $D_1$  and  $D_2$  in Fig. 6, were turned off so that the primary uncollided ion beam was also detected. These primary peaks appear near 910 eV with an energy spread similar to that observed in Fig. 5 for the argon support-gas ions. The neutral peaks, corresponding to the charge-exchanged neutral atoms from the gas cell, appear at about 934 eV, which is also consistent with the “sheath potential dc offset” seen in Fig. 5. These neutral peaks, after background subtraction, are shown expanded in the Fig. 7 inset. Note that a shift in primary beam energy between the 1 and 2 mTorr scans (from 910 to 912 eV) is reflected in a similar shift in the corresponding neutral peaks as expected. The 2-eV shift in primary beam energy between these energy scans is believed due to slight differences in the ion gun’s anode-to-plasma potential as the gun filament aged.

In order to determine the number of neutrals which were ionized and detected, the neutral peaks on the energy

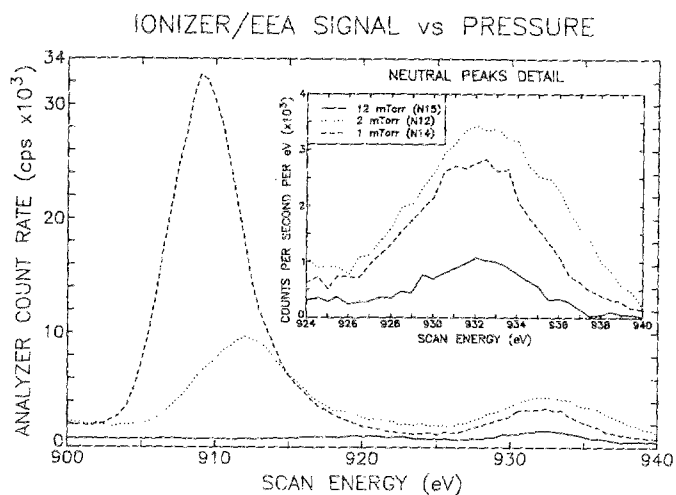


FIG. 7. Energy scans of charge-exchanged hydrogen beam at various gas cell pressures and (inset) expanded detail of neutral peaks.

scan were integrated over the peak width (924 to 940 eV) for the two distributions at 1 and 2 mTorr. The detection system efficiency, or the number of neutrals detected divided by the number incident, was  $7.2 \pm 2.6 \times 10^{-4}$  and  $5.8 \pm 1.9 \times 10^{-4}$  for the 1 and 2 mTorr energy scans, respectively. The relatively large error bars in these efficiency estimates were due primarily to uncertainties in the cross sections obtained for the charge exchange interaction in the gas cell. These results compared favorably with theoretical estimates for the ionizer efficiency, based on typical values for  $T_e$ ,  $N_e$ , and elastic scattering in the discharge support gas, of  $2.6 \pm 0.9 \times 10^{-4}$ . At lower neutral-flux energies, these efficiencies should increase proportional to  $E^{-1/2}$ .

## V. DISCUSSION

This paper has outlined the design, construction, and proof-of-principle verification of a neutral-hydrogen flux detection system, based on an ECRH discharge as the neutral ionizer. The significant aspects of the ionizer were its small size and excitation of the ECRH mode using relatively small static magnetic fields. The ionizer efficiency was experimentally determined for  $\approx 900$ -eV incident neutral hydrogen, using a calibration technique based on measured angle-dependent charge exchange cross sections. The successful calibration of the ionizer bodes well for its extension to lower-energy applications because the ionizer efficiency scales inversely with incident neutral-atom velocity. This work has established an experimental foundation for the exploration of low-energy ion/surface interactions through the demonstrated ability to detect low-intensity neutral-hydrogen fluxes. The detection system and associated hardware will be utilized for reflected neutral-flux measurements, and has potential for application in other areas such as fundamental cross-section measurement, plasma diagnostics, and beam/plasma interactions.

## ACKNOWLEDGMENTS

This research was made possible by fellowship support (B. L. Cain) of the Magnetic Fusion Energy Technology

Fellowship Program, Oak Ridge Associated Universities, Oak Ridge, TN, and by the National Science Foundation's Presidential Young Investigators Program (D. N. Ruzic). The authors also wish to thank B. Hu and R. A. Lindley, University of Illinois, for their technical assistance in the apparatus construction and testing, and express their appreciation to L. Stalker, University of Illinois, for his technical advice and talent in component fabrication.

- <sup>1</sup>G. M. McCracken and P. E. Stott, *Nucl. Fusion*, **19**, 889 (1979).
- <sup>2</sup>R. A. Langley, J. Bohdansky, W. Eckstein, P. Mioduszewski, J. Roth, E. Taglauer, E. W. Thomas, H. Verbeek, and K. L. Wilson, "Data Compendium for Plasma/surface Interactions: Special Issue 1984," *J. Plasma Phys. Thermonuclear Fusion*, IAEA, Vienna (1984).
- <sup>3</sup>H. Verbeek and the ASDEX Team, *J. Nucl. Mater.* **145-147**, 523 (1987).
- <sup>4</sup>S. M. Rosnagel, J. J. Cuomo, and W. D. Westwood, *Handbook of Plasma Processing Technology* (Noyes, Park Ridge, NJ, 1990).
- <sup>5</sup>D. N. Ruzic, D. B. Heifetz, and S. A. Cohen, *J. Nucl. Mater.* **145-147**, 527 (1987).
- <sup>6</sup>W. Eckstein and D. B. Heifetz, *J. Nucl. Mater.* **145-147**, 332 (1987).
- <sup>7</sup>W. Eckstein and J. P. Biersack, *Z. Phys. B* **63**, 109 (1986).
- <sup>8</sup>D. N. Ruzic and H. K. Chiu, *J. Nucl. Mater.* **162-164**, 904 (1989).
- <sup>9</sup>M. I. Baskes, *J. Nucl. Mater.* **128-129**, 676 (1984).
- <sup>10</sup>R. Aratari and W. Eckstein, *J. Nucl. Mater.* **162-164**, 910 (1989).
- <sup>11</sup>D. E. Post and R. Behrisch, *Physics of Plasma-Wall Interactions in Controlled Fusion*, NATO ASI Series B: Physics Vol. 131 (Plenum, New York, 1986).
- <sup>12</sup>B. L. Cain, "Analysis of Low Energy Neutral Hydrogen Fluxes Using an Electron Cyclotron Resonance Heated Discharge," Ph.D. thesis, Department of Nuclear Engineering, University of Illinois, October 1989.
- <sup>13</sup>H. Oechsner, W. Ruhe, and E. Stumpe, *Surf. Sci.* **85**, 289 (1979).
- <sup>14</sup>H. W. Werner and P. R. Boudewijn, *Vacuum* **34**, 83 (1984).
- <sup>15</sup>H. Oechsner and W. Gerhard, *Surf. Sci.* **44**, 480 (1974).
- <sup>16</sup>L. Wahlin, *Nucl. Instrum. Methods* **27**, 55 (1964).
- <sup>17</sup>M. Menzinger and L. Wahlin, *Rev. Sci. Instrum.* **40**, 102 (1969).
- <sup>18</sup>B. L. Cain, D. N. Ruzic, and R. Bastasz, *J. Vac. Sci. Technol. B* **6**, 485 (1988).
- <sup>19</sup>F. F. Chen, *Introduction to Plasma Physics* (Plenum, New York, 1977).
- <sup>20</sup>D. J. Rose and M. Clark, Jr., *Plasma and Controlled Fusion* (Wiley, New York, 1961).
- <sup>21</sup>M. A. Heald and C. B. Wharton, *Plasma Diagnostics with Microwaves* (Wiley, New York, 1965).
- <sup>22</sup>R. A. Helliwell, *J. Geophys. Res.* **61**, 139 (1956).
- <sup>23</sup>MACOR, Machinable Glass Ceramic, Code 9658, Corning Glass Works, Corning, NY 14830.
- <sup>24</sup>S. Dushman, *Scientific Foundations of Vacuum Technique* (Wiley, New York, 1949).
- <sup>25</sup>J. F. O'Hanlon, *A User's Guide to Vacuum Technology* (Wiley, New York, 1980).
- <sup>26</sup>D. J. Kroon, *Electromagnets* (N. V. Philips' Gloeilampenfabrieken, Eindhoven, The Netherlands, 1968).
- <sup>27</sup>E. M. Purcell, *Phys. Rev.* **54**, 818 (1938).
- <sup>28</sup>R. D. Birkhoff, *Nucl. Instrum. Methods* **8**, 313 (1960).
- <sup>29</sup>G. C. Theodoridis and F. R. Paolini, *Rev. Sci. Instrum.* **40**, 621 (1969).
- <sup>30</sup>Comstock Incorporated, "Operator's Manual: Double Focusing Electrostatic Energy Analyzer," Oak Ridge, TN, 1986.
- <sup>31</sup>R. J. Warmack, J. A. D. Stockdale, and R. N. Compton, *Int. J. Mass Spectrosc. Ion Phys.* **27**, 239 (1978).
- <sup>32</sup>J. L. Wiza, *Nucl. Instrum. Methods* **162**, 587 (1979).
- <sup>33</sup>P. Lecomte and V. Perez-Mendez, *IEEE Trans. Nucl. Sci.* **NS-25**, 964 (1978).
- <sup>34</sup>J. L. Wilson, J. B. O. Caughman II, Phi Long Nguyen, and D. N. Ruzic, *J. Vac. Sci. Technol. A* **7**, 972 (1989).
- <sup>35</sup>R. T. C. Tsui, *Phys. Rev.* **168**, 107 (1968).
- <sup>36</sup>M. J. Kushner, *J. Appl. Phys.* **58**, 4024 (1985).
- <sup>37</sup>R. H. Huddlestone and S. L. Leonard, *Plasma Diagnostic Techniques* (Academic, New York, 1965).
- <sup>38</sup>B. L. Cain, "Electric Probe Data Analysis for Glow Discharge Diagnostics," Master's Thesis, Department of Nuclear Engineering, University of Illinois, January 1987.